
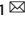


ARTICLE OPEN



Deciphering the involvement of the Hippo pathway co-regulators, YAP/TAZ in invadopodia formation and matrix degradation

Jubina Balan Venghateri¹, Bareket Dassa², David Morgenstern³, Michal Shreberk-Shaked⁴, Moshe Oren⁴  and Benjamin Geiger¹ 

© The Author(s) 2023

Invadopodia are adhesive, actin-rich protrusions formed by metastatic cancer cells that degrade the extracellular matrix and facilitate invasion. They support the metastatic cascade by a spatially and temporally coordinated process whereby invading cells bind to the matrix, degrade it by specific metalloproteinases, and mechanically penetrate diverse tissue barriers by forming actin-rich extensions. However, despite the apparent involvement of invadopodia in the metastatic process, the molecular mechanisms that regulate invadopodia formation and function are still largely unclear. In this study, we have explored the involvement of the key Hippo pathway co-regulators, namely YAP, and TAZ, in invadopodia formation and matrix degradation. Toward that goal, we tested the effect of depletion of YAP, TAZ, or both on invadopodia formation and activity in multiple human cancer cell lines. We report that the knockdown of YAP and TAZ or their inhibition by verteporfin induces a significant elevation in matrix degradation and invadopodia formation in several cancer cell lines. Conversely, overexpression of these proteins strongly suppresses invadopodia formation and matrix degradation. Proteomic and transcriptomic profiling of MDA-MB-231 cells, following co-knockdown of YAP and TAZ, revealed a significant change in the levels of key invadopodia-associated proteins, including the crucial proteins Tks5 and MT1-MMP (MMP14). Collectively, our findings show that YAP and TAZ act as negative regulators of invadopodia formation in diverse cancer lines, most likely by reducing the levels of essential invadopodia components. Dissecting the molecular mechanisms of invadopodia formation in cancer invasion may eventually reveal novel targets for therapeutic applications against invasive cancer.

Cell Death and Disease (2023)14:290; <https://doi.org/10.1038/s41419-023-05769-1>

INTRODUCTION

Tumor metastasis is a complex multi-step process that accounts for the vast majority of all cancer-related deaths [1, 2]. The metastatic invasion process is commonly initiated by the loss of intercellular cohesion in the primary tumor, followed by an invasion of the cancer cells, individually or collectively, into the surrounding tissues [3]. The invasive phase of the metastatic process, whereby the cancer cells penetrate into the nearby extracellular matrix (ECM) and blood vessels, utilizes tightly-coordinated adhesive-proteolytic-protrusive processes, combining integrin-mediated adhesion to the ECM, secretion of matrix metalloproteinases, and activation of cytoskeleton-based protrusive machinery that physically penetrate the surrounding connective tissue [4]. Throughout this process, the metastatic cancer cells sense the properties of the ECM and respond to the chemical and physical cues that eventually guide them to the neighboring vasculature [4].

The mechanical pressure applied by invading cells to the nearby matrix is generated by different membrane protrusions (e.g., filopodia, lamellipodia, ruffles, and invadopodia), the most

prominent of which are invadopodia that contain an integrin-based ECM adhesion domain, a protrusive actin-rich core, and diverse proteinases that degrade the matrix [5–8]. Invadopodia were first identified over 30 years ago in embryonic fibroblasts, transformed with Rous Sarcoma Virus [6, 9, 10], and later observed in a wide variety of cancers, including melanoma, head and neck tumors, as well as breast, pancreatic, and prostate carcinomas, to list just a few [11, 12]. Notably, some non-cancerous cells, such as dendritic cells, macrophages, endothelial cells, vascular smooth muscle cells, and osteoclasts, possess similar adhesion structures that are believed to partake in their physiological migratory and tissue remodeling activities [6, 13].

The invadopodia structural core comprises F-actin and several cytoskeleton-modulating and scaffolding proteins (e.g., cortactin, Tks4, Tks5, Wiskott-Aldrich Syndrome Protein (N-WASP), specific adhesion proteins (mainly integrins), as well as diverse signaling molecules, and their regulators (e.g., the cytoplasmic tyrosine kinase pp60Src, phosphoinositide 3-kinases) and different receptor tyrosine kinases, such as EGFR, PDGFR, and AXL [7, 14]. In addition, invadopodia contain various matrix-

¹Department of Immunology and Regenerative Biology, Weizmann Institute of Science, Rehovot, Israel. ²Bioinformatics Unit, Department of Life Sciences Core Facilities, Weizmann Institute of Science, Rehovot, Israel. ³de Botton Institute for Protein Profiling, The Nancy and Stephen Grand Israel National Center for Personalized Medicine, Weizmann Institute of Science, Rehovot, Israel. ⁴Department of Molecular Cell Biology, Weizmann Institute of Science, Rehovot, Israel. [✉]email: benny.geiger@weizmann.ac.il Edited by Professor Massimiliano Agostini

Received: 26 October 2022 Revised: 21 March 2023 Accepted: 23 March 2023

Published online: 25 April 2023

degrading proteases such as MT1-MMP (MMP14), MMP2, and MMP9 [6, 15].

Interestingly, despite the central involvement of invadopodia in the metastatic process and the vast effort invested in their characterization, the molecular mechanisms underlying their formation and activation are still poorly understood. Particularly challenging are the processes whereby cancer cells sense their microenvironment and respond to its chemical and mechanical properties (e.g., its rigidity) by activating the signaling networks that trigger invadopodia formation. Recent studies suggested, somewhat indirectly, the involvement of the Hippo-signaling pathway in invadopodia formation. For example, Amotl2 (the angiomin family member angiomin-like-2) was shown to localize to podosomes and invadopodia, where it modulates the organization of the actin cytoskeleton [13, 16]. Interestingly, Amotl2 was also shown to regulate the Hippo-signaling pathway by interacting with its transcription co-activator YAP [17]. In mammals, core components of this serine/threonine kinase signaling cascade include MST1 and MST2 and the large tumor suppressor kinases (LATS1 and LATS2) that suppress the activity of the transcriptional activators YAP and TAZ [18]. YAP/TAZ was shown to act as “mechanosensing switches” that respond to the chemical and physical properties of the cell microenvironment by modulating cellular activity and fate [19, 20]. Likewise, invadopodia were shown to interact with the ECM via specific integrin receptors [5–8] and to be affected by the rigidity of the underlying matrix [21]. Yet, specific information on the involvement of the Hippo pathway in invadopodia formation and activity is limited and mostly indirect. YAP was shown to localize to invadopodia in Src-transformed NIH-3T3 fibroblasts [22], though its involvement in the invasive process remains unclear and lacks mechanistic insights. Direct involvement of YAP through a nucleotide exchange factor TIAM1 was recently described [23].

In this study, we explored the possible roles of YAP and TAZ in invadopodia formation and invadopodia-mediated ECM degradation. Towards this aim, we initially screened a panel of 21 cultured cancer cell lines to check their capacity to form invadopodia *in vitro* and degrade the underlying gelatin ECM. Suppression of YAP, TAZ or both in most of the invadopodia-forming cell lines within this panel enhanced invadopodia formation and function. A similar effect was obtained when these cells were treated with the YAP/TAZ inhibitor verteporfin. Conversely, overexpression of either YAP, TAZ, or both, effectively blocked gelatin degradation. To identify specific invadopodia-associated components that are affected by YAP and TAZ suppression, we conducted proteomic and transcriptomic profiling of MDA-MB-231 breast cancer cells, that demonstrated the most prominent enhancement of invadopodia following YAP/TAZ depletion. Analysis of the proteomic data revealed that 94 proteins were differentially expressed upon the co-knockdown of YAP/TAZ. Among these, nine invadopodia-associated proteins showed significant changes, including an increase in the key core invadopodia components Tks5 and MMP14, which are essential for invadopodia formation [24–27]. Furthermore, transcriptome analysis identified 18 differentially expressed invadopodia-related genes following the co-knockdown of YAP/TAZ in the same cells. Overall, these results show that YAP and TAZ act as negative regulators of invadopodia formation and matrix degradation in multiple cancer cell lines, suggesting a regulatory role for these transcriptional co-activators in cancer invasion and metastasis.

MATERIALS AND METHODS

Fluorescence microscopy reagents

Primary antibodies used in this study included; rabbit monoclonal antibody anti-YAP/TAZ (D24E4; Cell Signaling Technology, Catalog No-

8418), rabbit polyclonal anti-TKS5 antibody (Santa Cruz Biotechnology, Catalog No: SC-7390), and rabbit polyclonal anti-TKS5 antibody (Merck, Catalog No: 09-403). Secondary antibodies used here included; peroxidase-conjugated goat anti-mouse IgG (Jackson ImmunoResearch Laboratories, Catalog No: 115-035-003), peroxidase-conjugated goat anti-rabbit IgG (Jackson ImmunoResearch Laboratories, Catalog No: 111-035-144), and goat anti-rabbit IgG Alexa Fluor647 (Thermo Fisher Scientific, Catalog No: A32728). F-actin was stained using Phalloidin-tetramethylrhodamine B isothiocyanate (Sigma Aldrich, Catalog No: P1951). Nuclei were stained using 4',6-diamidino-2-phenylindole dihydrochloride (DAPI; Sigma Aldrich-Aldrich, Catalog No- D9542).

Cultured cell lines used in this study

Cancer cell lines purchased from the American Type Culture Collection (ATCC) include MDA-MB-231, NCI-H1299, A375, SKOV-3, OVCAR-3, A549, PC3, PANC-1, MDA-MB-468, A2780, HCC1937, and HCC70. Melanoma cell lines 63T, WM793, CSK-A375, and A2058 were sourced as previously described [28]. Cell lines IGR-1, LOX-IMVI, and Malme-3M were kindly provided by Prof. Yarden Samuels (Weizmann Institute of Science, Rehovot, Israel). UM-SCC-47 line was a kind gift from Dr. Itay Tirosh (Weizmann Institute of Science, Rehovot, Israel). Melanoma cell line SB-2 was a kind gift from Prof. Menashe Bar-Eli (The University of Texas MD Anderson Cancer Center, Houston, TX, USA). Cancer cell lines MDA-MB-231, A375, CSK-A375, WM793, A2058, 63T, IGR-1 LOX-IMVI, SB-2, Malme-3M, SKOV-3, OVCAR-3, A549, PC3, PANC-1, MDA-MB-468 and A2780 were cultured in DMEM, supplemented with 10% FCS (Gibco) 2 mM glutamine, 2 mM NEAA, and 100 U/mL penicillin–streptomycin. Cell lines NCI-H1299, HCC1937, and HCC70 were cultured in an RPMI medium containing 10% FCS (Gibco), 2 mM glutamine, 2 mM NEAA and 100 U/mL penicillin–streptomycin. UM-SCC-47 cell line was cultured in three parts of Hams F-12 nutrient mixture medium and one part of DMEM with 10% FCS (Gibco) and 100 U/mL penicillin–streptomycin. All cell lines were maintained at 37 °C under a humidified atmosphere of 5% CO₂ and 95% air. All cell lines were routinely tested for mycoplasma using the mycoplasma detection kit, MycoAlert™ (Lonza Nottingham, Ltd). Frozen vials of cell stock were thawed, and cells were cultured for no more than a month for the experiments. Additional information on all the cell lines used in this study is summarized in Table S1.

Transfection procedures

Knockdown experiments. Transfection was performed using siGENOME Human YAP1 siRNA, SMART pool; M-012200-00-0005 and siGENOME Human WWTR1 (TAZ) siRNA, SMART pool; M-016083-00-0005, siGENOME Human SH3PXD2A (TKS5) siRNA, SMART pool; M-006657-02-0005 and siGENOME Human MMP14 siRNA, SMART pool; M-004145-00-0005 (GE Healthcare Dharmacon). siRNA non-targeting pool #2 (GE Healthcare Dharmacon) was used as a control for all the knockdown experiments. The SMART pool and single oligo siRNA sequences used for the experiments are enlisted in the supplementary Tables S2 and S3. The final concentration for each siRNA was 30 nmol/L. The siRNAs were transfected using DharmaFect transfection reagent, according to the manufacturer's protocol. Fresh medium was added after 6 h to replace the medium with transfection reagent and oligonucleotides. Cells were incubated for 48 h following the siRNA transfection and proceeded for further experiments.

Overexpression experiments. IRES-GFP empty vector was sourced as previously described [28]. pcDNA Flag-YAP1 and pcDNA3 Flag-TAZ were obtained as described previously [29]. Tks5 RFP plasmid construct was kindly provided by Sara A. Courtneidge (School of Medicine, Oregon Health & Science University, Portland, OR, USA). MMP14 plasmid-pCMV3-SP-N-Flag was procured from Sino Biological (Catalog No: HG10741-NF). Flag-YAP1 and Flag-TAZ were transfected using the jetPEI transfection reagent (Polyplus-Transfection®) according to the manufacturer's instructions. The plasmids were purified using Qiagen Maxi Kit and quantified using a Nanodrop spectrophotometer (Thermo Fisher Scientific, Catalog No: ND-2000). Briefly, MDA-MB-231 and NCI-H1299 (0.7×10^6) cells were seeded on a 10 cm cell culture dish and incubated for 24 h. Subsequently, the cells were transfected with empty vector, Flag-YAP1, Flag-TAZ, and Flag-YAP1 plus Flag-TAZ. The final concentration of each plasmid used for overexpression was 10 µg per 10 cm culture dish. For Flag-YAP1 plus Flag-TAZ condition, the total concentration was 20 µg per 10 cm cell culture dish. The cells were then incubated for 48 h before proceeding with further experiments.

Preparation of gelatin-coated culture plates

The matrix degradation activity of cancer cell lines, tested in this study, was conducted using 2D and rigid tissue culture surfaces to which fluorescently tagged gelatin was covalently bound. The gelatin coating of coating of plates for the matrix degradation assay was conducted as previously described [28]. Briefly, 96 micro-well plates, with a glass-bottom (Thermo Fisher Scientific Catalog No-164588) were treated with 50 mg/mL of poly-L-lysine (Sigma Aldrich, Catalog No-P-4707) prepared as 1:1 mixture with Dulbecco's Phosphate Buffered Saline (DPBS, Biological Industries, Catalog No-02-023-1A) and incubated for 20 min at room temperature. Then, the poly-lysine solution was removed, and the plate was washed ($\times 3$) with DPBS. Porcine skin gelatin (Sigma Aldrich, catalog no. G2500) was prepared in DPBS (2 mg/mL) and filtered through a 0.22-micron Steritop filter (Millipore Fisher Scientific Catalog No-15770319). Gelatin was fluorescently labeled using Alexa Fluor 488 Protein labeling kit (Molecular Probes, Thermo Fisher Scientific) according to the manufacturer's instructions. The gelatin was subsequently cross-linked using N-(3-Dimethylaminopropyl)-N'-ethylcarbodiimide hydrochloride (EDC hydrochloride) (Sigma Aldrich Catalog No-03450) and N-Hydroxysuccinimide (NHS) (Sigma Aldrich Catalog No-130672), prepared as 10% solutions in ddH₂O. Subsequently, 96-well glass-bottom plates were coated with 40 μ L volume of a mixture (10:1) of unlabeled gelatin and the Alexa Fluor 488 labeled gelatin. For every 100 μ L gelatin, the gelatin to cross-linker mixture ratios was (82.5 μ L gelatin: 12.5 μ L NHS: 5 μ L EDC). Subsequently, the gelatin mixture was incubated for 1 h at room temperature. After incubation, the surfaces of the gelatin-coated plates were washed three times with DPBS. One hundred microliters of fresh DPBS solution was added to the wells and UV sterilized for 30 min in the biosafety hood. The plates were then ready to use.

Gelatin degradation assay

The different cancer cell lines (10^4) were seeded on the Alexa Fluor 488-labeled gelatin matrix in the 96-well plates and cultured for 5–6 h. The cells were then fixed and stained for F-actin and DAPI, washed with DPBS, and kept wet for imaging. Every experiment was performed in two or more replicate wells for each condition. Z-stack of images was acquired using a WiScan[®] Hermes Automated High Content Imaging System (IDEA Bio-Medical Ltd) using 40 \times /0.75 NA air objective. In a single well, images from a total of 36 fields were acquired, and the cells were counted based on the nuclear (DAPI) staining. The degraded gelatin area (μm^2 per cell) was calculated using the Image J software (rsbweb.nih.gov/ij). All degradation values following treatments were compared to those of control cells cultured on the same plate in every independent set of experiments.

The effect of EGF stimulation on gelatin degradation

Cancer cell lines (SKOV-3 and OVCAR-3) were grown in a medium containing 10% FBS and serum-starved (0.5% FBS) for 24 h. Subsequently, cells that were cultured in 0.5% FBS were stimulated with hEGF (recombinant EGF) (Sigma Aldrich, Catalog No: E9644) in concentrations (10 and 30 ng/mL) and plated on Alexa 488-gelatin for 5–6 h. The cells were then processed for the gelatin degradation assay as described above.

The effect of YAP/TAZ inhibitor verteporfin on gelatin degradation

For gelatin degradation, an assay measuring the effect of the YAP/TAZ inhibitor verteporfin (Holland Moran, Catalog No 1711461), MDA-MB-231 and NCI-H1299 cells were seeded on the Alexa Fluor 488-labeled gelatin matrix and cultured for 2 h. Subsequently, the cells were treated either with vehicle (0.1% DMSO) or with different concentrations of verteporfin (final concentration range: 0.5–20 μ M) for 4 h. The cells were then fixed and stained for TRITC-Phalloidin and DAPI and imaged using a WiScan[®] Hermes Automated High Content Imaging System (IDEA Bio-Medical Ltd) under 10 \times /0.75 NA air objective.

Immunostaining, microscopy, and image analysis

Cells (10^4 /well) were seeded on the Alexa Fluor 488-tagged gelatin in 96-well glass-bottom plates. At the end of the gelatin degradation experiment (usually 5–6 h after plating) the cells were fixed and permeabilized for 3 min with 3% PFA, 0.5% Triton-X-100, in DPBS followed by 3% PFA for another 30 min. Then, the cells were washed ($\times 3$) with DPBS and incubated with the primary antibody for 1 h. Subsequently, the cells were washed with DPBS ($\times 3$) and incubated

with the appropriate secondary antibody for 30 min. The cells were washed again ($\times 3$) with DPBS and kept in DPBS for imaging. The images were acquired using a DeltaVision Elite microscopy system, equipped with a microtiter stage (Applied Precision Inc., Issaquah, WA) with 40 \times /0.75 air or 60 \times /1.42 oil objectives (Olympus). All acquired images were analyzed using Image J software (<https://imagej.nih.gov/ij/>).

Cell viability assay

A microscopy-based cell viability assay was performed as previously described [30]. Hoechst 33342 (1 μ g/mL; ImmunoChemistry Technologies, Bloomington, MN, USA) and propidium iodide (250 ng/mL; Sigma Aldrich, St. Louis, MO, USA) in DMEM were added onto cells and kept in the 37 $^{\circ}$ C incubator for 45 min. The cells were centrifuged at 1200 rpm for 3 min and then proceeded for imaging. The images were acquired using a WiScan Hermes[®] microscope with a 10 \times objective (IDEA Bio-Medical Ltd), and the percentage of live and dead cells was calculated using WiSoft[®] Athena software (IDEA Bio-Medical Ltd).

Western blot analysis

Cells plated on a 10 cm cell culture dish were scraped using a cell scraper and suspended in 300 μ L ice-cold RIPA buffer. The cell lysates were kept on ice and vortexed at 5-min intervals for over 45 min. Then, the lysates were cleared by centrifugation at 274 $\times g$ at 4 $^{\circ}$ C for 10 min. The cell lysates were either freshly examined or stored at -80° C. The frozen samples were thawed on ice, subjected to 10% polyacrylamide/SDS gel electrophoresis, and subsequently blotted onto Polyvinylidene fluoride (PVDF) membrane (Merck Millipore[®] Catalog No IPVH00010). The blots were blocked using 5% skimmed milk in Tris Buffered Saline, containing Tween 20, pH 8.0 (TBST) buffer, and probed with primary antibody overnight at 4 $^{\circ}$ C. They were then washed with TBST buffer $\times 3$ (10 min each) and incubated with HRP-coupled secondary antibody (Jackson ImmunoResearch Laboratories Inc.) for 1 h. Chemiluminescent Super Signal West Pico substrate (Thermo Fisher Scientific, Catalog number: 34579) was used for detecting the bands, and the blots were imaged using ChemiDoc MP Imager and quantified using Image Lab 4.1 software (BioRad, USA).

Quantitative real-time PCR

RNeasy Mini Kit (Catalog No-74104; Qiagen) was used for isolating total RNA from cells. Total RNA (1–2 μ g) was reverse-transcribed using LunaScript[™] RT SuperMix Kit (New England Biolabs, Catalog No; E3010S). Quantitative real-time RT-PCR (qRT-PCR) was performed using a Fast SYBR Green Master Mix using the OneStep instrument (Applied Biosystems). The obtained values were normalized to either HPRT1 or GAPDH genes. The primers used for the experiments are enlisted in Supplementary Table S4.

Preparation of cells for proteomic profiling

For knockdown experiments, MDA-MB-231 (0.7×10^6) cells were seeded on 10 cm cell culture dishes, incubated for 24 h, transfected with siControl, siYAP, siTAZ, and a mixture of siYAP and siTAZ SMARTpools, and further incubated for 48 h. The YAP/TAZ knockdown cells were seeded on unlabeled gelatin-coated 10 cm plates and cultured at 37 $^{\circ}$ C for 5–6 h. The effect of the treatment on the cells' gelatin degradation activity was verified, in parallel, by plating a sample of the same cells on Alexa Fluor 488-gelatin plates and measuring their gelatin degradation phenotype. The experimental design consisted of three independent set of experiments for each knockdown condition. The cells were washed with 5 mL cold PBS and then scraped into 1 mL fresh ice-cold PBS, centrifuged at 3000 rpm at 4 $^{\circ}$ C, and the cell pellets were flash-frozen in liquid nitrogen and stored at -80° C.

Sample preparation for proteomic analysis

Frozen cell pellet samples were dissolved in 5% SDS, 50 mM Tris-HCl (pH 7.5) The total protein concentration was measured using a BCA assay. 100 μ g of each sample was used for the downstream preparation. Dithiothreitol (DTT) was prepared fresh in 50 mM ammonium bicarbonate, and added to a final concentration of 5 mM. The samples were then incubated at 56 $^{\circ}$ C for 1 h. Iodoacetamide was prepared fresh in 50 mM ammonium bicarbonate, and was added to final concentration of 10 mM. Samples were incubated in the dark for 45 min. Phosphoric acid was then added to the samples to final concentration of 1%. The samples were mixed with 350 μ L of 90% methanol along with 10% 50 mM

ammonium bicarbonate, then transferred to the S-trap filter and centrifuged for 1 min at $4000 \times g$ and washed 3 times with $400 \mu\text{L}$ of 90% MeOH + 10% 50 mM ammonium bicarbonate, then centrifuged at $4000 \times g$ 1 min. $4 \mu\text{L}$ of $0.5 \mu\text{g}/\mu\text{L}$ Trypsin in $125 \mu\text{L}$ in ammonium bicarbonate (25:1 protein amount: trypsin) was added to the samples. Samples were incubated at 37°C overnight. The next day, peptides were eluted using $80 \mu\text{L}$ 50 mM ammonium bicarbonate, which was added to the S-trap cartridge, centrifuged at $4000 \times g$ for 1 min into new tubes, and collected the peptides. Then, a second digestion was performed using $4 \mu\text{L}$ of $0.5 \mu\text{g}/\mu\text{L}$ trypsin in 50 mM ammonium bicarbonate was added to the eluted samples and incubated at 37°C for 4 h. Two more elutions from the S-trap cartridge were performed. One with $80 \mu\text{L}$ of 0.2% formic acid, which was added to the S-trap cartridge and spun down at $4000 \times g$ for 1 min. The second was done using $80 \mu\text{L}$ of 50% acetonitrile + 0.2% formic acid was added to the cartridge and spun down at $4000 \times g$ for 1 min. The three elutions were mixed and dried using a vacuum centrifuge (Centrivac, LabConco).

Proteomic analysis

The resulting peptides were analyzed using a nanoAcquity liquid chromatography (Waters) coupled with a Q Exactive HF-X (Thermo fisher scientific). Samples were analyzed randomly, loaded on a Symmetry C18 trap column ($20 \text{ mm} \times 0.18 \text{ mm}$, $5 \mu\text{m}$, Waters), and resolved on a HSS T3 ($250 \text{ mm} \times 0.075 \text{ mm}$, $1.8 \mu\text{m}$, Waters) analytical column at $350 \text{ nL}/\text{min}$, using a gradient of 4–27%B (MeCN, 0.1% formic acid) for 155 min. MS1 acquisition was performed at m/z range of $375\text{--}1650$ at $120,000$ resolution ($@400 \text{ m/z}$), allowing Automatic Gain Control (AGC) target of 10^6 with a maximum Injection Time (IT) of 60 ms. MS2 acquisition was performed on the Top10 ions at Data-Dependent Acquisition (DDA) using Higher-energy Collisional Dissociation (HCD) fragmentation set at 27 Normalized Collision Energy (NCE) acquired at $15,000$ resolution ($@200 \text{ m/z}$). IT was set to 60 ms and AGC to $1e5$. Dynamic exclusion was set to 30 s with a counter of 1. The resulting data was processed with MaxQuant (v1.6.6.0). The data were searched with the Andromeda search engine against the Human proteome database (SwissProt Nov20) appended with common lab protein contaminants. The following modifications were allowed: fixed carbamidomethylation on C, variable protein N-terminal acetylation, variable deamidation on NQ and variable oxidation on M. The quantification was based on the LFQ method, based on unique peptides.

Bioinformatics analysis

For each cancer cell line used in this study (See Supplementary Table S1), we retrieved the information concerning the tissue of origin (e.g., primary tumor vs. metastases) from the CCLE database (<https://depmap.org/portal/download/>). Bioinformatic analysis of the proteomic data of MDA-MB-231 cells was applied on LFQ intensities of 4704 detected proteins. Proteins having at least two one razor and unique peptides were considered, and 37 known contamination were removed from the analysis. For the detection of differential proteins, intensities were \log_2 transformed and analyzed with ANOVA following a multiple test correction (FDR step-up) using Partek Genomics Suite 7.0. For each pairwise comparison, we considered proteins having at least two valid measurements (out of 3) in both groups and that passed the thresholds of fold change $|(\log_2)| > 1$ and p value < 0.16 . In addition, proteins that were detected in at least 2 replicates in one group and completely absent in the other group were also considered as qualitatively differential proteins. For visualization of the protein expression, heat maps were prepared using Partek Genomics Suite, using \log_2 -transformed LFQ intensities with row standardization (scaling the means of a row to zero, with a standard deviation of 1), and partition clustering using the k-means algorithm (Euclidian method). For volcano plot visualization, missing values were imputed to a value of 15, and new fold change values were calculated with ANOVA and visualized using MATLAB. Principle component analysis (PCA) was calculated using Partek Genomics Suite. For visualization of proteins network, the relations between differential proteins of the double knockdown was inferred with StringDB [31] as a "full STRING network", and visualized by Cytoscape 3.7.2 [32]. The width of the edges corresponds to the "combined score" or StringDB, and the protein color scale corresponds to their \log_2 fold change as inferred from the proteomics ANOVA. Proteins that change qualitatively (were detected only in one condition) were assigned an imputed value of ± 5 . The assignment of proteins belonging to Hippo signaling, cell adhesion, and ECM remodeling

pathways was inferred using the GeneCards suite [33]. A list of invadopodia-related proteins was compiled by data mining in the Harmonizome database and the related literature [34–43].

RNA sequencing

MDA-MB-231 cells (0.7×10^6) were seeded on 10 cm culture dishes and incubated for 24 h. Subsequently, the cells were transfected with SMARTpool siRNA for siControl, siYAP, siTAZ, and siYAPTAZ and incubated for a further 48 h for the knockdown. After the incubation, the knockdown cells were seeded on non-labeled gelatin-coated 10 cm plates and cultured for 5–6 h in an incubator. Subsequently, the culture medium was aspirated, and the cells were given a wash with DPBS. One milliliter of DPBS was added to the plate, and the cells were then scraped using a cell scraper. Then the cells were centrifuged at 3000 rpm at 4°C . The supernatant was aspirated, and the RNA was extracted from the cell pellet. The RNA extraction was done using RNeasy Mini Kit (Catalog Nos; 74104, 74106 Qiagen) according to the manufacturer's instructions. The RNA was quantified using Qubit 3 Fluorometer (ThermoFisher scientific, USA) and TapeStation (Agilent Technologies 4200, USA) to assess the purity of RNA. A RIN (RNA Integrity Number) score ranging from 9–10 was obtained for each condition. Then RNA-seq libraries were prepared at the Crown Genomics institute of the Nancy and Stephen Grand Israel National Center for Personalized Medicine, Weizmann Institute of Science. Libraries were prepared using the INCPM-mRNA-seq protocol. Briefly, the polyA fraction (mRNA) was purified from 500 ng of total input RNA followed by fragmentation and the generation of double-stranded cDNA. Afterwards, Agencourt Ampure XP beads cleanup (Beckman Coulter), end repair, A base addition, adapter ligation and PCR amplification steps were performed. Libraries were quantified by Qubit (Thermo fisher scientific) and TapeStation (Agilent). Sequencing was done on a NovaSeq6000 instrument (Illumina) using an SP 100 cycles kit (single read sequencing).

Transcriptomic analysis

RNA sequencing analysis was done using the UTAP transcriptome analysis user-friendly Transcriptome Analysis Pipeline (UTAP v1.10) transcriptome analysis pipeline (Kohen, Barlev et al. 2019). Reads were trimmed to remove adapters and low quality bases using cut adapt (-a "A pipeline") [44]. Reads were trimmed to remove adapters and low quality bases using cut adapt (-a "A (10)" -a "T (10)" -times 2 -q 20 -m 25) [45] and mapped to the human genome (GRCh38, GENCODE version 34) using STAR v2.4.2a [46] (using-alignEndsType EndToEnd, -outFilterMismatchNoverlmax. 0.05, -two pass Mode Basic). Reads were counted using STAR, and genes having minimum of five reads in at least one sample were considered. Normalized counts and detection of differential expression were performed using DESeq2 [47] (betaPrior, cooksCutoff, and independent filtering parameters set to False). Differentially expressed genes were selected with absolute fold change (\log_2) ≥ 1 and adjusted multiple testing p value ≤ 0.05 [48]. Matlab was used to generate the volcano plots.

Statistical analysis

All statistical analysis of the experimental data was performed using the Graph Pad Prism version 8.0.1 for Windows, GraphPad Software, San Diego, CA, USA, www.graphpad.com software. Statistical significance for each experiment is marked in the form of asterisks (*) along with the calculated p value for experiments are shown.

RESULTS

Differential gelatin degradation and invadopodia formation by a panel of cultured cancer cell lines

Towards the selection of cultured cancer cell lines that would be suitable for testing the involvement of the Hippo pathway in invadopodia formation and matrix degradation, we assembled a panel of 21 cancer cell lines (See Supplementary Table S1). These lines were derived from the following cancers: melanomas (A375, CSK-A375, A2058, WM793, 63-T, IGR-1, Malme-3M, SB-2, LOX-IMVI); breast carcinoma (MDA-MB-231, MDA-MB-468, HCC1937, HCC70); head and neck squamous cell carcinoma (UM-SCC-47); non-small cell lung carcinoma (NCI-H1299); lung adenocarcinoma (A549); ovarian carcinoma (SKOV-3, OVCAR-3, A2780); prostate carcinoma (PC3) and pancreatic cancer (PANC-1). For details on the tissue of

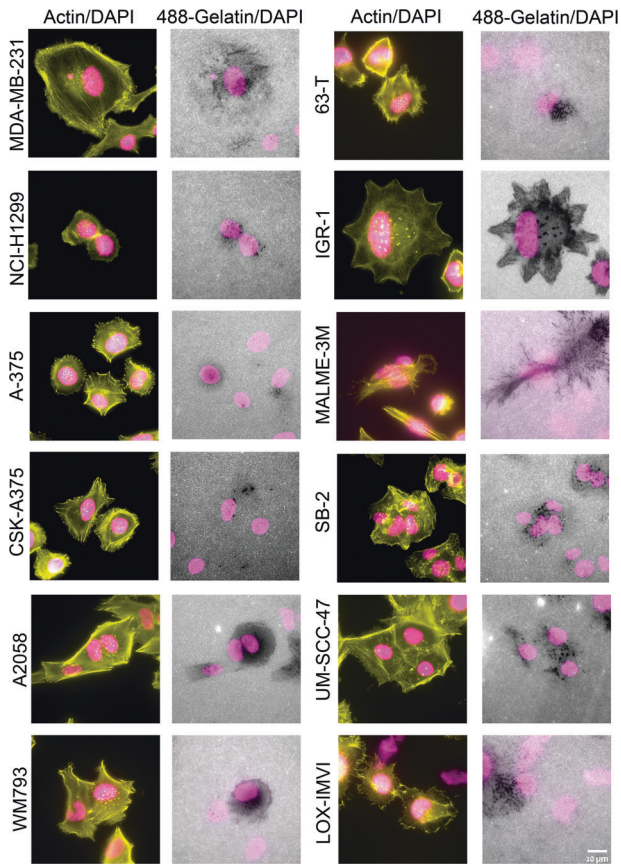


Fig. 1 A panel of multi-cancer cell lines screened for gelatin degradation and actin-rich invadopodia structures. Cell lines were cultured on a fluorescently labeled (488) gelatin and cultured for 5–6 h. Subsequently, the cells were fixed and stained for actin (TRITC-phalloidin) and DAPI. Images were acquired under 60 \times /1.42 oil objective. Among the 21 multi-cancer cell line panel used in the study, 12 cancer cell lines (shown here) were found to be positive for the actin-rich invadopodia appearing as prominent actin-rich dots near the nucleus and gelatin matrix degradation. Scale bar is 10 μ m.

origin, site of isolation (primary tumor vs. metastasis), and capacity to degrade gelatin matrix, see Supplementary Table S1. Imaging of the gelatin degradation by the 21 tested cell lines revealed considerable diversity in their basal gelatin degradation and invadopodia formation capacity. Specifically, 12 cell lines display a significant and consistent gelatin degradation activity with an average gelatin degradation score $>1 \mu\text{m}^2/\text{cell}$ (Fig. 1). Quantification of the gelatin degradation by these cell lines pointed to high variability, ranging from an average degradation score of $3 \mu\text{m}^2/\text{cell}$ to over $100 \mu\text{m}^2/\text{cell}$ (Fig. 2). It is noteworthy that the 12 “degradation-positive” cell lines were originally derived from melanoma (9/9), breast cancer (1/4), NSCLC (1/1), and squamous cell carcinoma (1/1). Furthermore, all the gelatin degrading cell lines formed conspicuous actin-rich invadopodia, often overlapping with the degraded areas (dark spots) on the gelatin matrix (Fig. 1 and “zoomed-in” images of IGR-1 and SB-2 cells, shown in Supplementary Fig. S1). The nine-cell lines that displayed low or no gelatin degradation ($<1 \mu\text{m}^2/\text{cell}$) included those derived from ovarian cancer (3/3), breast cancer (3/4), lung adenocarcinoma (1/1), pancreatic carcinoma (1/1), and prostate carcinoma (1/1), (Supplementary Fig. S2). Attempts to stimulate invadopodia formation in of two of these nine “invadopodia-negative” cancer cell lines (SKOV-3 and OVCAR-3) using EGF (10 and 30 ng/mL), see also [49] or YAP/TAZ suppression (see below) did not trigger

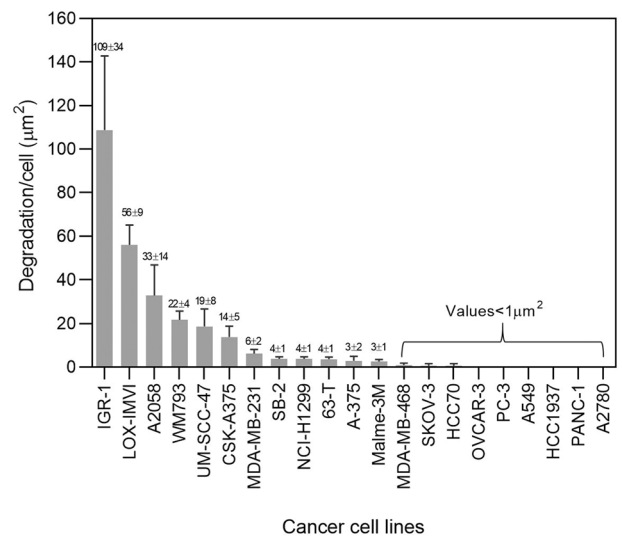


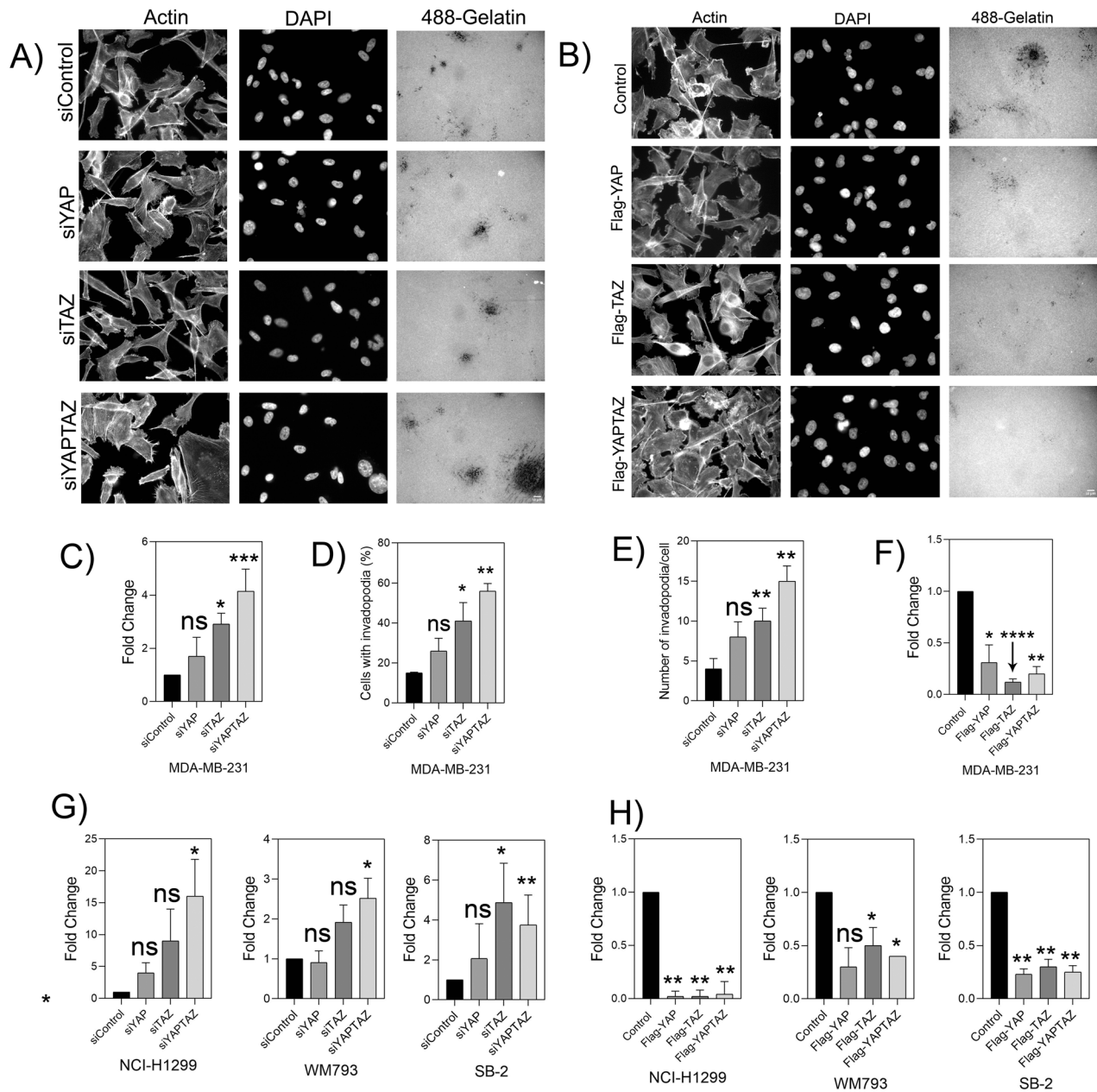
Fig. 2 Quantitation of gelatin matrix degradation in a multi-cancer cell line panel. Cells were seeded on FITC labeled gelatin matrix and cultured for 5–6 h. Subsequently, the cells were fixed with 3% paraformaldehyde in PBS and stained for actin and DAPI. Each cell line was seeded in duplicate wells. Images were acquired using 40 \times /0.75 air objective. 36 fields were imaged per well and the gelatin degradation/cell (μm^2) was quantitated using ImageJ software. The plot shows the average of four independent data sets with \pm SEM. The p value was found to be (<0.0001). Four independent sets of experiments were performed and the average plot is shown. These cell lines then served as platform for further experiments in this study.

enhanced invadopodia formation or gelatin degradation in these cells (Supplementary Fig. S3).

Depletion or inhibition of YAP and TAZ in a subset of invadopodia-forming cancer cell lines, enhances invadopodia formation and gelatin degradation

To investigate the involvement of the Hippo pathway in invadopodia formation and function, we subjected the entire panel of the 21 cancer cell lines (both those scored positive and those scored negative for matrix degradation and invadopodia formation) to siRNA-mediated knockdown of YAP, TAZ or both (SMARTpool siRNAs are listed in Table S2). As shown in Supplementary Fig. S4, the 9 cell lines that displayed average gelatin degradation levels below $1 \mu\text{m}^2/\text{cell}$ remained negative also after YAP and TAZ knockdown and were not further tested in this study.

We then proceeded with testing the effect of YAP/TAZ knockdown on the cell lines that displayed a basal level of matrix degradation, starting with MDA-MB-231 cells. The efficient knockdown of YAP and TAZ in these cells at both mRNA (Supplementary Fig. S5A) and protein (Supplementary Fig. S5B) levels was confirmed, and off-target effects were excluded by the use of individual siRNA duplexes (sequences in Supplementary Table S3). The effect of YAP/TAZ suppression in these cells on the gelatin degradation score is shown in Supplementary Fig. S6. Quantifying these results pointed to a significant increase in matrix degradation following the knockdown of both YAP and TAZ (about 4-fold). Suppression of either YAP or TAZ yielded a more modest yet consistent elevation of matrix degradation (Fig. 3A and quantified in Fig. 3C). We further confirmed that YAP and TAZ knockdown led to over 3-fold increase in the percentage of invadopodia-forming cells (Fig. 3D) and a similar increase in number of invadopodia per cell (Fig. 3E). The quantification of actin-rich invadopodia was based on supervised segmentation of phalloidin-labeled cells (see Materials and Methods). To further confirm that the segmented actin-rich dots are indeed bona fide invadopodia, we labeled the



cells for Tks5, a highly specific invadopodia component. A comparison of the actin labeling and the Tks5 labeling confirmed that the actin-rich structures are genuine invadopodia (Fig. 4).

Similar trends, albeit with varying intensities, were also observed in the other cancer cell lines, primarily NCI-H1299, WM793 and SB-2 (Fig. 3G), and partially in UM-SCC-47 (Supplementary Fig. S7). Notably in most of the tested lines, suppression of TAZ displayed stronger effect on invadopodia, that that of YAP, and maximal increase in invadopodia formation and degradation activity were obtained upon suppression of both YAP and TAZ. Other cell lines (e.g. A375, CSK-A375, A2058) were not affected by YAP/TAZ suppression (Supplementary Fig. S7). The results presented in Fig. 3 and Supplementary Fig. S7 were obtained from 300–400 cells/condition, and indicated a significant increase in the percentage of invadopodia containing cells in NCI-H1299 (siControl-26%, siYAP-37%, siTAZ-49%, siYAPTAZ-50%) WM793 (siControl-69%, siYAP-79%, siTAZ-84%, siYAPTAZ-88%), SB-2

(siControl-37%, siYAP-45%, siTAZ-51%, siYAPTAZ-59%) respectively. In addition, we noticed a significant increase in the average number of invadopodia in those cells (NCI-H1299: siControl- 8 ± 2 , siYAP- 10 ± 3 , siTAZ- 19 ± 5 , siYAPTAZ- 23 ± 3 ; WM793: siControl- 18 ± 4 , siYAP- 20 ± 4 , siTAZ- 25 ± 6 , siYAPTAZ- 42 ± 5 ; SB-2: siControl- 14 ± 2 , siYAP- 17 ± 5 , siTAZ- 26 ± 5 , siYAPTAZ- 34 ± 5).

As a complementary approach to YAP/TAZ downregulation, we treated the cells with verteporfin, a potent inhibitor of YAP and TAZ [50, 51]. Exposure of MDA-MB-231 cells for 6 h to increasing concentrations of verteporfin (0.5–20 μ M) had no apparent effect on cell viability. However, treatment with 10 and 20- μ M verteporfin resulted in a 3- and 9-fold elevation, respectively, in the gelatin degradation activity (Fig. 5). This further supports the notion that YAP and TAZ suppress invadopodia formation and matrix degradation. Together these experiments show that both YAP and TAZ have a capacity to suppress invadopodia-mediated matrix degradation.

Fig. 3 Knockdown of YAP/TAZ elevates gelatin matrix degradation and invadopodia formation in MDA-MB-231. A YAP/TAZ was knocked down for 48 h using SMART pool siRNA. The knockdown cells were then seeded on Alexa Fluor 488-labeled gelatin matrix and cultured for 5–6 h. Cells were fixed and stained for actin and DAPI. Z-stack of images for actin, DAPI and Alexa Fluor 488-gelatin were captured under 40× (0.75) air objective using a WIScan Hermes® microscope (IDEA Bio-Medical Ltd). Four independent set of experiments were performed. A representative panel of the captured images are shown. Scale bar is 10 µm. **B** Cells were overexpressed with empty vector control, Flag-tagged YAP, TAZ and YAP + TAZ plasmids and incubated on Alexa Fluor 488-gelatin for 5–6 h. Cells were fixed and stained for actin and DAPI. Z-stack of images for actin, DAPI and Alexa Fluor 488-gelatin were captured under 40× (0.75) air objective using a WIScan Hermes® microscope (IDEA Bio-Medical Ltd). Four independent set of experiments were performed. A representative panel for the images of one of the set is shown. Scale bar is 10 µm. **C** Fold change obtained from the values for gelatin degradation/cell (µm²) is plotted for each treatment condition. The significance values calculated by paired *t* test was (Control vs siYAP) ns, not significant, (Control vs siTAZ) **P* value < 0.00330, (Control vs siYAP + TAZ) ****P* value < 0.0008. The *P* value was **** < 0.0001 by one-way ANOVA for treatment conditions when compared to control. **D** An average plot (Mean ± SEM) of percentage of cells with invadopodia counted for each treatment condition is shown. The significance values for the treatment conditions as calculated by paired *t* test was (Control vs siYAP) ns, not significant, (Control vs siTAZ) **P* value < 0.0039, (Control vs siYAP + TAZ) ***P* value < 0.0021. *P* value was *, 0.0251 for treatment conditions when compared to control as determined by one-way ANOVA. **E** An average plot (Mean ± SEM) of number of invadopodia/cell counted for each treatment condition. The significance values for the treatment conditions as calculated by paired *t* test was (Control vs siYAP) ns, not significant, (Control vs siTAZ) ***P* value < 0.0032, (Control vs siYAP + TAZ) ***P* value < 0.0020. *P* value was *, 0.0116 for treatment conditions when compared to control as determined by one-way ANOVA. **F** An average plot of gelatin degradation/cell (µm²) with (Mean ± SEM) for each treatment condition after overexpression of YAP, TAZ or both is shown. The significance values for the treatment conditions as calculated by paired *t* test was (Control vs siYAP) *, 0.0264, (Control vs siTAZ) ****, *P* value < 0.0001, (Control vs siYAP + TAZ) **, *P* value < 0.0019. *P* value was *, 0.0197 for treatment conditions when compared to control as determined by one-way ANOVA. **G** Fold change obtained from the values for gelatin degradation/cell (µm²) for different cancer cell lines after knockdown of YAP, TAZ or both are shown. Data is average (Mean ± SEM) of three independent sets of experiments. (NCI-H1299- ns, not significant, **P* value 0.0146 for treatment conditions when compared to control as determined by one-way ANOVA), WM793-*, *P* value 0.0040 for treatment conditions when compared to control as determined by one-way ANOVA, SB-2-* *P* value 0.0197, **, 0.0052 for treatment conditions when compared to control as determined by one-way ANOVA, UM-SCC-47-*** *P* value 0.004, * *P* value 0.0153, ** 0.0023 for treatment conditions when compared to control and as determined by one-way ANOVA. **H** Fold change obtained from the values for gelatin degradation/cell (µm²) for different cancer cell lines after overexpression with YAP, TAZ or both are shown. Data is average (Mean ± SEM) of four independent sets of experiments. (NCI-H1299-**, *P* value 0.0082 for treatment conditions when compared to control as determined by one-way ANOVA), WM793-*, *P* value 0.00373 for treatment conditions when compared to control as determined by one-way ANOVA, SB-2-**, *P* value 0.0041 for treatment conditions when compared to control as determined by one-way ANOVA, UM-SCC-47 ns, not significant, * *P* value 0.0148, * *P* value 0.0305 for treatment conditions when compared to control as determined by one-way ANOVA after overexpression with YAP, TAZ or both are shown.

Overexpression of YAP and TAZ suppresses extracellular matrix degradation

The results presented above, indicating an increase in invadopodia following YAP/TAZ suppression, suggest, indirectly, that these molecules suppress invadopodia-mediated matrix degradation. To substantiate this notion, we overexpressed Flag-tagged YAP, TAZ, or both in the vast majority of the invadopodia-forming lines (MDA-MB-231, NCI-H1299, WM793, SB-2, A375, CSK-A375, A2058, UM-SCC-47, LOX-IMVI, MALME-3M), and tested the effect of the overexpression on invadopodia activity (Western blot validation of the expression of YAP and TAZ is shown in Fig. S5C). As shown in Fig. 3B and quantified in Fig. 3F, H, overexpression of YAP, TAZ, and particularly both together, led to a substantial reduction in gelatin degradation as compared to the empty vector control. In addition, overexpression of YAP, TAZ or both significantly reduced the percent invadopodia-forming cells and the number of invadopodia/cell in the tested cell lines.

Testing of the effect of YAP/TAZ overexpression on invadopodia formation in cells that displayed poor or no response to YAP/TAZ suppression is presented in Supplementary Fig. 7. As shown, those cells that were not affected by YAP/TAZ suppression (A375, CSK-A375, A2058), were not affected by the overexpression of these molecules. UM-SCC-47, that displayed enhanced response to knockdown of YAP and YAP + TAZ (but not of TAZ) alone, was effectively suppressed by overexpression of YAP, TAZ and both (Supplementary Fig. 7). Invadopodia formation in LOX-IMVI and MALME-3M was not suppressed by overexpression (Supplementary Fig. S7) Overall, our results indicate that YAP and TAZ inhibit invadopodia formation in multiple cancer cell lines.

Proteomic profiling of YAP/TAZ knockdown in MDA-MB-231 cells

To identify downstream molecular targets underlying the apparent suppressive effect of YAP and TAZ on invadopodia

formation and degradation, we conducted proteomic profiling in MDA-MB-231 cells, which showed the most prominent results. Specifically, the samples subjected to the proteomic analysis consisted of three independent sets of experiments involving: (1) untransfected control cells; (2) siControl (“transfection control”), (3) siYAP, (4) siTAZ, (5) siYAP + siTAZ. This proteomic profiling yielded quantitative data for 4667 proteins (see Supplementary Table S5). Principal component analysis (PCA) of the data revealed that, overall, the control groups (siControl) could be well separated (with PC1) from the sample groups (siYAP, siTAZ, siYAP + TAZ) and that the double knockdown was clearly separated from the single knockdown replicates (Supplementary Fig. S8A). Differences in protein expression between the experimental groups were evaluated with ANOVA, using thresholds as described in “Materials and methods”. Comparison of the analyses of the “non-transfected” and siControl-transfected cells resulted in only a few (16) differential proteins between the two control groups, suggesting that the transfection might have a small, negligible effect. Thus, further analyses of the knockdown effects were conducted by comparing the siControl and the “Hippo-suppressed” groups (siYAP, siTAZ, siYAP + siTAZ). Altogether, the proteomic profiling analysis detected 122 proteins that were differentially affected upon silencing of either YAP (29 proteins) or TAZ (27 proteins), and a more pronounced effect was detected upon co-knockdown of YAP + TAZ (94 proteins, Supplementary Table S6 and Supplementary Fig. S9). A Venn diagram showing the overlap of differentially expressed proteins in each condition is shown in Supplementary Fig. S10. Among the differentially expressed proteins in the double knockdown were proteins known to be involved in the Hippo-signaling pathway, such as TGFB2, AJUBA, FRMD6, YAP1, SERPINE1, and proteins associated with cell adhesion and ECM remodeling pathways (e.g., SERPINE1, THBS1, COL6A1, MMP14, TIMP3, LAMA5, ITGB5). These results support the role of the Hippo pathway in molecularly regulating ECM degradation.

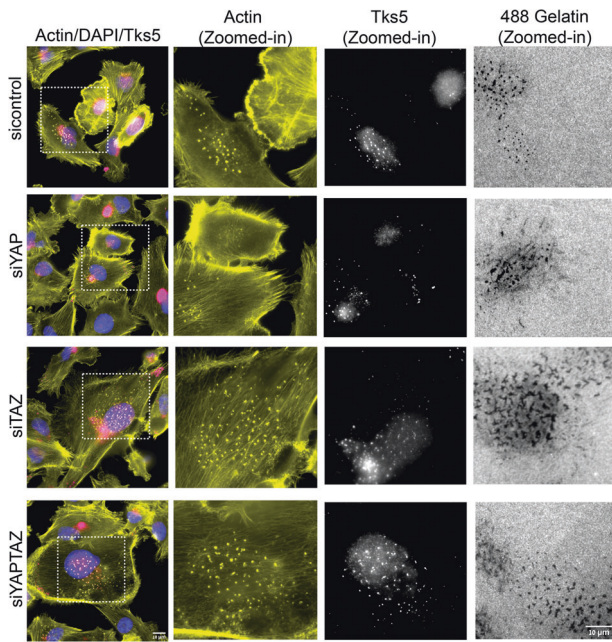


Fig. 4 Knockdown of YAP, TAZ or YAP + TAZ in MDA-MB-231 causes elevation in gelatin degradation and invadopodia. MDA-MB-231 cell lines were knockdown for siControl, siYAP, siTAZ and siYAP+TAZ and incubated on Alexa Fluor 488-gelatin for 5–6 h. Cells were fixed and stained for actin, DAPI, and invadopodia-specific marker Tks5. Cells in the first panel are marked with dotted line white boxes displaying actin (yellow), Tks5 dots (white) and corresponding dark gelatin degradation areas as zoomed-in images are shown.

YAP and TAZ modulate the levels of key invadopodia-associated proteins

To determine whether knockdown of YAP + TAZ affects the levels of invadopodia-associated proteins, we compiled a list of proteins associated with invadopodia structure and functionality (Supplementary Table S7). The list was primarily based on the scientific literature [35, 40–42], the *Harmonizome* database [34], and selected proteomic reports [36–39, 43]. Given that these resources are based on data obtained by different methods, diverse cell types, and that association with invadopodia (e.g., structural, functional, and regulatory) was not strictly and uniformly defined, our list is rather comprehensive, albeit with limited editing. This crude list comprises diverse proteins, including membrane receptors, cytoskeletal proteins, adapter proteins, proteinases, and other enzymes, along with the components of different signaling networks. Notably, co-knockdown of YAP and TAZ in the MDA-MB-231 cell line revealed significant differential expression of nine invadopodia-associated proteins (Fig. 6). Of those, seven proteins (ADAM19, DIAPH2, GSN IDH1, ITGB5, MMP14 (MT1-MMP), and SH3PXD2A (commonly referred to as Tks5)) were upregulated whereas two proteins (SERPINE1 and AKAP12) were down-regulated. The majority of these proteins are known to play key roles in invadopodia formation, matrix degradation, matrix adhesion and organization of the actin cytoskeleton (see Figs. 6, 7 and Supplementary Table S8).

To directly validate the mechanistic relevance of YAP/TAZ-mediated suppression of TKS5 and MMP14 levels on invadopodia activity in MDA 231 cells, we have tested the effect of knockdown each of these invadopodia-associated proteins, or both on the gelatin degradation levels in untreated or siYAP + TAZ-knockdown cells. As shown in the Supplementary Fig. S11A knockdown of YAP + TAZ in MDA-MB-231 cells increased invadopodia activity 3.8

fold, consistent with Fig. 3. Co-suppression of either TKS5 or MMP14 in both untreated and siYAP + TAZ completely abolished the gelatin degradation by the cells, indicating that each of these two invadopodia components is essential for invadopodia activity, both in the presence or absence of YAP and TAZ. We further tested if both TKS5 and MMP14 can restore invadopodia activity in YAP + TAZ overexpressing cells. As shown in Supplementary Fig. S11B, overexpression of YAP + TAZ suppressed invadopodia activity, consistent with Fig. 3. Overexpression of TKS5 or MMP14 in untreated MDA-MB-231 cells increased gelatin degradation by 5.5 ± 1 and 4.6 ± 0.3 -fold, respectively. Interestingly, overexpressing TKS5 in YAP + TAZ overexpressing cells restored invadopodia activity, while MMP14 failed to restore gelatin degradation.

To determine whether the changes in the invadopodia-associated proteome described here were regulated at the transcriptional or the post-transcriptional levels, we conducted transcriptome profiling after co-knockdown of YAP and TAZ in MDA-MB-231 cells (Supplementary Table 9). PCA analysis of the RNA sequencing results showed good separation between the siControl group and the treated groups (siYAP, siTAZ, siYAP+TAZ) (Fig. S8B). Similar to the protein profiling results, a more pronounced differential effect of YAP + TAZ knockdown on gene expression was observed, affecting 580 genes. The majority of these genes were affected only when the expression of both YAP and TAZ was suppressed, whereas a single knockdown of YAP affected 34 genes and that of TAZ 61 genes (Supplementary Fig. S12). Out of these YAP + TAZ-affected genes, 18 had a documented association with invadopodia, including 5 integrin chains, matrix metalloproteinases, matrix components, signaling molecules, and cytoskeletal regulators. Notably, only gelsolin appeared in both the proteomic and the transcriptomic lists of differentially affected invadopodia-related proteins (Supplementary Table 10). Hence, YAP and TAZ are affecting invadopodia formation via multiple regulatory mechanisms.

DISCUSSION

The involvement of the Hippo-signaling pathway in cancer development, progression, and metastasis, has attracted considerable interest in recent years [19, 52, 53]. Yet the nature of its effects on the diverse manifestations of the malignant phenotype in cancer-derived cells lines, as well as in cell subpopulations within tumors (e.g. deregulated growth, aberrant apoptotic and metabolic properties, enhanced migratory activity and invasiveness) remains highly complex and often controversial [54, 55]. For example some reports related to the general involvement of YAP/TAZ in cancer formation, refer to these molecules as oncogenes [18, 56], while others suggest that they molecules act as tumor suppressors [54, 55, 57]. The results presented in this paper reflect a complex relationship between the acquisition of invasive phenotype in vivo or ex vivo, and invadopodia formation. Our initial survey of multiple cell lines for invadopodia formation revealed an unexpected cell line-specific diversity. Specifically, among the 21 cell lines tested, 12 displayed a basal invadopodia formation, and 9 lines that do not form invadopodia in our ex vivo experimental system. Incidentally, to our knowledge, this is the first and largest comparative characterization of matrix degradation competence of multiple cancer cell lines. Interestingly, the majority of the lines that fail to form invadopodia, were reported to display metastatic potential in vivo (e.g. SKOV-3 OVCAR-3, A2780 [58], A549 [59], PANC-1 [60], PC3 [61], MDA-MB-468, HCC70, HCC1937 [62]). Moreover, even among the invadopodia-forming cells – the experimental modulation of YAP and/or TAZ (both knockdown and overexpression) led to diverse effects, suggesting that invadopodia formation can be regulated via multiple and different cell-specific signaling pathways. In about half of these cell lines (e.g. MDA-MB-231, H1299, WM793, SB-2 and, partly, UM-SCC-47) these Hippo regulators appear to play key suppressive

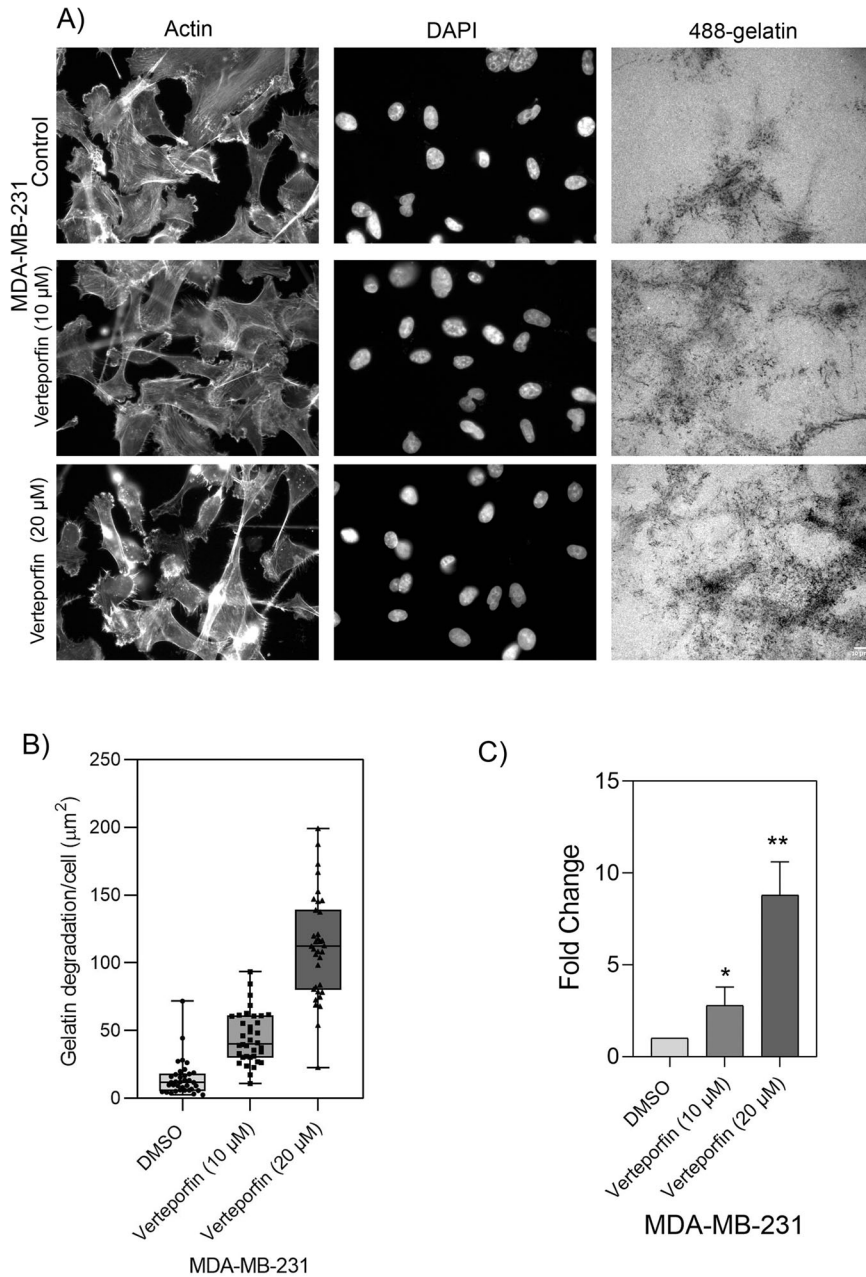


Fig. 5 Verteporfin inhibitor causes elevation in gelatin degradation in MDA-MB-231 cell line. MDA-MB-231 cell line was treated with vehicle control, 10 and 20 μM of verteporfin and incubated for 5–6 h on Alexa 488-labeled gelatin. Z-stack of images for actin, DAPI and Alexa Fluor 488-gelatin were captured under $40\times(0.75)$ air objective using a WIScan Hermes[®] microscope (IDEA Bio-Medical Ltd). Four independent set of experiments were performed. **A** A representative panel of images for each treatment condition are shown. Scale bar is 10 μm . **B** An average plot of gelatin degradation/cell (μm^2) with \pm SEM for each treatment condition is shown. **C** Fold change obtained from the values for gelatin degradation/cell (μm^2) is plotted for each treatment condition. The significance values for the treatment conditions was calculated by two-tailed *t* test. ***P* value < 0.0033, **P* value < 0.0408. *P* value < 0.0012 (**) as determined by one-way ANOVA.

role in invadopodia formation, while in other cellular systems YAP/TAZ suppression or overexpression did not consistently affect invadopodia formation and the main regulatory system remains unclear (Supplementary Fig. S7). In view of variable response to YAP/TAZ modulation, we have focused our study on the YAP/TAZ responsive lines, aiming to decipher the molecular mechanism underlying this regulatory process.

We would like to emphasize that while our primary screen was based on morphological examination of the gelatin degradation, the cells were further checked for the formation of actin-rich

invadopodia, showing that cells that failed to degrade the matrix were, largely, devoid of invadopodia (Fig. S2). Multi-color fluorescence microscopy further validated that the structures identified as invadopodia indeed contain TK5, an invadopodia-specific adaptor protein that often co-localizes with gelatin-degradation sites (Fig. 4 and Supplementary Fig. 1). Notably, the co-localization of invadopodia with the locally degraded matrix is partial, due to the dynamic nature of invadopodia formation and turnover. Interestingly, essentially all the cell lines, derived from melanoma cancers (9/9, derived either from metastases or primary tumors) formed

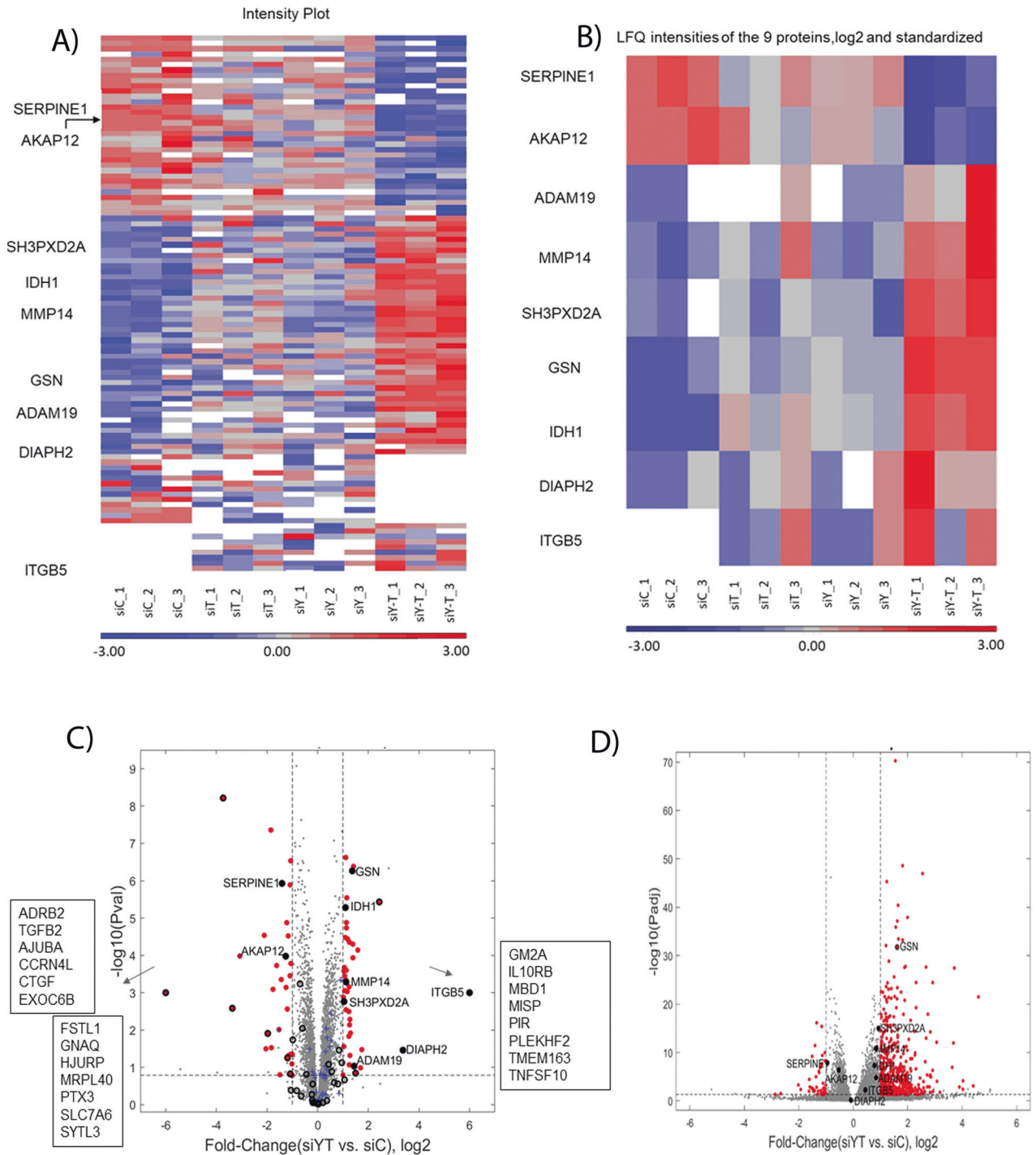


Fig. 6 Protein profiling results after knockdown of YAP, TAZ or both in MDA-MB-21 cell line. **A** A heatmap of the expression levels of 122 differential proteins obtained from the proteomic profiling for each treatment condition with three independent sets of experiments are shown. LFQ intensities were log2 transformed and standardized. Missing values are shown in white. **B** A heatmap of the nine invadopodia-related proteins that were differentially expressed proteins after co-knockdown of YAP + TAZ. **C** Volcano plot from protein profiling results showing significantly differential proteins marked as red dots indicating up-regulation of proteins such as ADAM19, DIAPH2, GSN, IDH1, ITGB5, MMP14 (MT1-MMP), SH3PXD2A on the right side whereas downregulation of proteins AKAP12 and SERPINE1 on the left side. Proteins that changed qualitatively in the analysis are listed in boxes Blue crosses indicate hippo-signaling pathway proteins detected from the protein profiling results. Black empty circles denote proteins that were detected in the single knockdown of either YAP or TAZ. **D** Volcano plot for the genes obtained from the transcriptome analysis. Red dots indicate differentially expressed genes.

conspicuous invadopodia, while cell lines derived, for example, from ovarian adenocarcinomas or breast adenocarcinoma were mostly invadopodia negative (4/4 and 3/4, respectively). Further attempts to induce invadopodia formation and matrix degradation in the

invadopodia-negative cell lines, e.g., by changing the environmental conditions (e.g., EGF stimulation); see [49], or the cells' signaling machinery (e.g., knockdown of YAP and TAZ, inspired by the present study) failed to turn-on invadopodia formation in these cells,

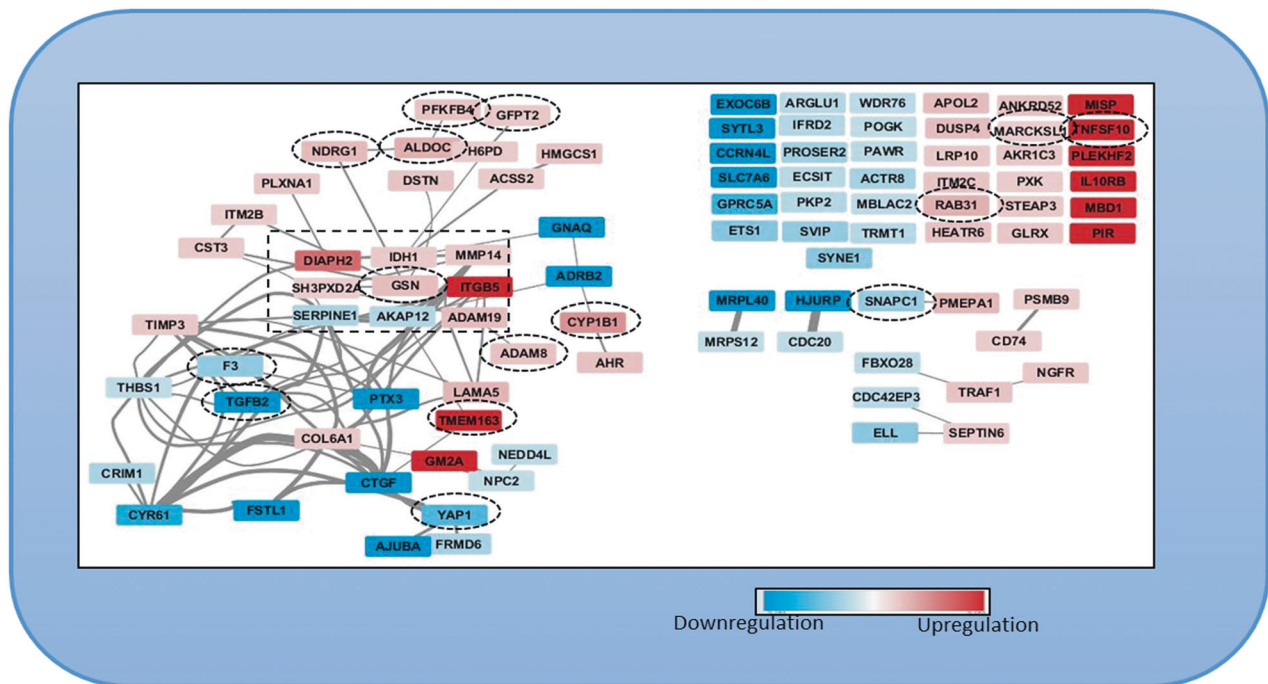


Fig. 7 Network of 94 invadopodia-specific proteins resulting from the protein profiling analysis after co-knockdown of YAP + TAZ in MDA-MB-231 cell line. Invadopodia-specific proteins that were upregulated (red) and downregulated proteins (blue) are shown. Sixty-three proteins had either functional or physical protein associations whereas 38 proteins did not have a known protein association. Proteins differentially expressed in both proteomics and transcriptomic profiling are encircled in black dotted boxes.

suggesting that these cells might use invadopodia-independent mechanisms for their invasion and dissemination, at least under culture conditions. Suppressing the expression of YAP, TAZ or both in the invadopodia-forming cells, had a variable effect on matrix degradation; cells displaying either high or modest gelatin degradation score (e.g. A2058, UM-SCC-47, LOX-IMVI, A375, CSK-A375, and 63-T), were not affected by YAP/TAZ or were partially suppressed, suggesting a Hippo-insensitive regulation of invadopodia in these cells. In contrast, a group of 4 cell lines (MDA-MB-231, H1299, WM793, and SB-2) displayed a pronounced and consistent elevation in invadopodia formation and gelatin degradation phenotype following YAP/TAZ knockdown (Fig. 3). Further, 2 cell lines (MALME-3M and UM-SCC-47) showed varying levels of elevation in invadopodia formation and gelatin degradation phenotype for single knockdowns of YAP or TAZ but co-knockdowns of both YAP/TAZ was consistent as the 4 cell lines (MDA-MB-231, H1299, WM793 and SB-2) described previously. This suggests that the Hippo pathway (via the inhibition of YAP and TAZ by MST/LATS) promotes invadopodia formation. This view is further corroborated by the enhancement of invadopodia after treating the cells with the YAP/TAZ signaling inhibitor verteporfin (Fig. 5) and by the suppression of invadopodia formation and activity following YAP/TAZ overexpression. Interestingly, contrary to the knockdown effects, which often exhibited differential effects of the two co-activators, whereby TAZ had a more robust effect on matrix degradation than YAP, The overexpression of each of them alone (and, certainly a combination of the two), had a comparable suppressive effect. This observation is consistent with the view that both YAP and TAZ suppress invadopodia and that the differential effect of their knockdown reflects variations in their relative prominence in the tested cell lines or their differential regulation by the Hippo core phosphorylation cascade [29].

The search for specific downstream targets affected by YAP and TAZ knockdown included, primarily, proteomic and transcriptomic analysis of differentially expressed molecules (siYAP+TAZ vs. siControl), focusing on invadopodia-related components. Towards that goal, we have assembled a literature-curated invadopodia

components database that contains structural and regulatory components of invadopodia and the associated cytoskeleton (Supplementary Table S7). Towards that end, we have identified the differentially expressed proteins and transcripts detected by the proteomic and mRNA profiling, respectively. Overall, the proteomic data revealed significant changes in the levels of 150 proteins (72 were upregulated and 78 downregulated). Further, for each knockdown conditions, the differentially expressed proteins were found to be siYAP vs siControl (29 proteins) or siTAZ vs siControl (27 proteins), and siYAP+siTAZ vs siControl (94 proteins). In addition, some proteins (28) were common because they were identified as differentially expressed in more than one knockdown condition. Excluding the 28 proteins that were common in each knockdown condition results in 122 unique proteins in the proteomic profiling results obtained. The RNA-seq data, showed differential expression of 675 transcripts (600 were upregulated and 75 downregulated). Further, for each knockdown conditions, the differentially expressed genes were found to be siYAP vs siControl (34 genes) or siTAZ vs siControl (61 genes), and siYAP +siTAZ vs siControl (580 genes) (Supplementary Table 10 and Supplementary Fig. S12). Notably, among the downregulated molecules were known direct downstream transcriptional targets of the Hippo pathway, including YAP1 CTGF, CYR61. Comparing the proteomic and transcriptomic lists of differentially expressed molecules revealed 15 overlapping components (F3, TGFB2, YAP1, SNAPC1, MARCKSL1, CYP1B1, TMEM163, PFKFB4, TNFSF10, GFPT2, NDRG1, GSN, ADAM8, ALDOC, RAB31; see Fig. 7), among which there was just one molecule (gelsolin), which is included in our invadopodia list. Further data mining of the functionality of the differentially expressed proteins strongly supported the notion that the 7 proteins that were significantly elevated following YAP + TAZ knockdown are essential invadopodia components. Specifically, TK55, an adaptor phospho-protein was shown to be essential for invadopodia formation, recruitment of proteases, matrix degradation, extravasation and tumor growth in vivo [25, 27, 63, 64]. MMP14, is a key protease required for

invadopodia-mediated matrix degradation [24], ADAM19 is a member of the ADAM family (A Disintegrin And Metalloprotease) [25, 65], which is involved in invadopodia formation. In addition, the formin family member DIAPH2 [66, 67], as well as integrin $\beta 5$ (together with different α -chains) form the adhesive-protrusive domains of invadopodia [68, 69]. It is noteworthy that gelsolin, an actin modulator associated with invadopodia [70, 71], was elevated both transcriptionally and proteomically. The role of IDH, in invadopodia formation and matrix degradation is still unclear at the mechanistic level [39] and will require further investigation. Two invadopodia-related proteins that were down-regulated following YAP + TAZ suppression were Serpine1 [72], which can affect matrix degradation, and AKAP12 [73], which affects PKA distribution in cells. The direct roles of these proteins in invadopodia-mediated cancer invasion is still unknown. Out of the 580 genes whose transcription was significantly affected by YAP/TAZ knockdown, 18 were present in our invadopodia-related list (Supplementary Table 10 and Supplementary Fig. S12), including several integrin chains, matrix metalloproteinases, actin-associated proteins, and signaling modulators. Our validation experiments, focusing specifically on TKS5 and MMP14, whose levels were significantly augmented upon YAP and TAZ suppression, confirmed that these invadopodia components indeed play a key role in the YAP/TAZ-mediated regulation of invadopodia activity. Specifically, the knockdown of TKS5 and MMP14 essentially abolished the enhancing effect of YAP/TAZ suppression. Moreover, overexpression of TKS5 restored invadopodia activity in MDA-MB-231, overexpressing YAP and TAZ. An unexpected and intriguing result was that, unlike TKS5, MMP14 overexpression failed to restore gelatin degradation in YAP + TAZ overexpressing MDA-MB-231 cells. We propose that TKS5 acts "upstream" to MMP14, and is capable of supporting invadopodia activity by recruiting other MMPs, like MMP2 and MMP9 [6].

Taken together, these results suggest that invadopodia formation and matrix degradation activity are regulated at multiple levels, transcriptional and post-transcriptional. The proteomic and transcriptomic data presented here, clearly demonstrate that YAP and TAZ suppress essential structural components of invadopodia and suggest that Hippo-mediated inhibition of YAP/TAZ may increase the invasive phenotype. Further studies are warranted to better understand the precise role of the different Hippo pathway mediators that affect the activity of YAP and TAZ, either as individual proteins or as paralogs. Dissecting their contextual behavior and clarifying their conflicting functions in different cancer cell types will eventually enable the design and application of novel therapies targeting cancer invasion and metastasis.

DATA AVAILABILITY

The raw data of proteomic profiling has been deposited at the ProteomeXchange via the Proteomic Identification Database (PRIDE partner repository). The dataset identifier ID is PXD034562. The accession numbers for the RNA-seq data have been deposited in NCBI's Gene Expression Omnibus [74] and are accessible through Genome Sequence Archive for Human under GEO Series accession number: GSE205726. There are no restrictions on the availability of the data.

REFERENCES

- Welch DR, Hurst DR. Defining the hallmarks of metastasis. *Cancer Res.* 2019;79:3011–27.
- Dillekas H, Rogers MS, Straume O. Are 90% of deaths from cancer caused by metastases? *Cancer Med.* 2019;8:5574–6.
- Gloushankova NA, Zhitnyak IY, Rubtsova SN. Role of epithelial-mesenchymal transition in tumor progression. *Biochem Biokhim.* 2018;83:1469–76.
- Kai F, Drain AP, Weaver VM. The extracellular matrix modulates the metastatic journey. *Dev Cell.* 2019;49:332–46.
- Aseervatham J. Cytoskeletal remodeling in cancer. *Biology.* 2020;9:385.
- Murphy DA, Courtneidge SA. The 'ins' and 'outs' of podosomes and invadopodia: characteristics, formation and function. *Nat Rev Mol Cell Biol.* 2011;12:413–26.
- Paz H, Pathak N, Yang J. Invading one step at a time: the role of invadopodia in tumor metastasis. *Oncogene.* 2014;33:4193–202.
- Revach OY, Grosheva I, Geiger B. Biomechanical regulation of focal adhesion and invadopodia formation. *J Cell Sci.* 2020;133:jcs244848.
- Chen WT. Proteolytic activity of specialized surface protrusions formed at rosette contact sites of transformed cells. *J Exp Zool.* 1989;251:167–85.
- Chen WT, Chen JM, Parsons SJ, Parsons JT. Local degradation of fibronectin at sites of expression of the transforming gene product pp60src. *Nature.* 1985;316:156–8.
- Linder S, Wiesner C, Himmel M. Degrading devices: invadosomes in proteolytic cell invasion. *Annu Rev Cell Dev Biol.* 2011;27:185–211.
- Luo Y, Hu J, Liu Y, Li L, Li Y, Sun B, et al. Invadopodia: a potential target for pancreatic cancer therapy. *Crit Rev Oncol/Hematol.* 2021;159:103236.
- Proszynski TJ, Gingras J, Valdez G, Krzewski K, Sanes JR. Podosomes are present in a postsynaptic apparatus and participate in its maturation. *Proc Natl Acad Sci USA.* 2009;106:18373–8.
- Revach OY, Geiger B. The interplay between the proteolytic, invasive, and adhesive domains of invadopodia and their roles in cancer invasion. *Cell Adhes Migr.* 2014;8:215–25.
- Hoshino D, Branch KM, Weaver AM. Signaling inputs to invadopodia and podosomes. *J Cell Sci.* 2013;126:2979–89.
- Proszynski TJ, Sanes JR. Amotl2 interacts with LLSbeta, localizes to podosomes and regulates postsynaptic differentiation in muscle. *J Cell Sci.* 2013;126:2225–35.
- Zhao B, Li L, Lu Q, Wang LH, Liu CY, Lei Q, et al. Angiotin is a novel Hippo pathway component that inhibits YAP oncoprotein. *Genes Dev.* 2011;25:51–63.
- Harvey KF, Zhang X, Thomas DM. The Hippo pathway and human cancer. *Nat Rev Cancer.* 2013;13:246–57.
- Dupont S, Morsut L, Aragona M, Enzo E, Giulitti S, Cordenonsi M, et al. Role of YAP/TAZ in mechanotransduction. *Nature.* 2011;474:179–83.
- Wada K, Itoga K, Okano T, Yonemura S, Sasaki H. Hippo pathway regulation by cell morphology and stress fibers. *Development.* 2011;138:3907–14.
- Jerrell RJ, Parekh A. Matrix rigidity differentially regulates invadopodia activity through ROCK1 and ROCK2. *Biomaterials.* 2016;84:119–29.
- Daszczuk P, Prószyński T. Hippo signaling pathway transcription-co-activator YAP is localized topodosomes/invadopodia in Src-transformed NIH-3T3 fibroblasts. *Matters.* 2016:2297–8240. <https://sosjournals.s3.amazonaws.com/ij3zDTIUM3G7Jvav.pdf>.
- Shen J, Huang Q, Jia W, Feng S, Liu L, Li X, et al. YAP1 induces invadopodia formation by transcriptionally activating TIAM1 through enhancer in breast cancer. *Oncogene.* 2022;41:3830–45.
- Ferrari R, Martin G, Tagit O, Guichard A, Cambi A, Voituriez R, et al. MT1-MMP directs force-producing proteolytic contacts that drive tumor cell invasion. *Nat Commun.* 2019;10:4886.
- Abram CL, Seals DF, Pass I, Salinsky D, Maurer L, Roth TM, et al. The adaptor protein fish associates with members of the ADAMs family and localizes to podosomes of Src-transformed cells. *J Biol Chem.* 2003;278:16844–51.
- Sharma VP, Eddy R, Entenberg D, Kai M, Gertler FB, Condeelis J. Tks5 and SHIP2 regulate invadopodium maturation, but not initiation, in breast carcinoma cells. *Curr Biol.* 2013;23:2079–89.
- Seals DF, Azucena EF Jr, Pass I, Tesfay L, Gordon R, Woodrow M, et al. The adaptor protein Tks5/Fish is required for podosome formation and function, and for the protease-driven invasion of cancer cells. *Cancer Cell.* 2005;7:155–65.
- Revach OY, Sandler O, Samuels Y, Geiger B. Cross-talk between receptor tyrosine kinases AXL and ERBB3 regulates invadopodia formation in melanoma cells. *Cancer Res.* 2019;79:2634–48.
- Shreberk-Shaked M, Dassa B, Sinha S, Di Agostino S, Azuri I, Mukherjee S, et al. A division of labor between YAP and TAZ in non-small cell lung cancer. *Cancer Res.* 2020;80:4145–57.
- Adutler-Lieber S, Friedman N, Geiger B. Expansion and antitumor cytotoxicity of T-cells are augmented by substrate-bound CCL21 and intercellular adhesion molecule 1. *Front Immunol.* 2018;9:1303.
- Szklarczyk D, Gable AL, Nastou KC, Lyon D, Kirsch R, Pyysalo S, et al. The STRING database in 2021: customizable protein–protein networks, and functional characterization of user-uploaded gene/measurement sets. *Nucleic Acids Res.* 2020;49:D605–D612.
- Shannon P, Markiel A, Ozier O, Baliga NS, Wang JT, Ramage D, et al. Cytoscape: a software environment for integrated models of biomolecular interaction networks. *Genome Res.* 2003;13:2498–504.
- Stelzer G, Rosen N, Plaschkes I, Zimmerman S, Twik M, Fishilevich S, et al. The GeneCards suite: from gene data mining to disease genome sequence analyses. *Curr Protoc Bioinform.* 2016;54:1.30.31–31.30.33.
- Rouillard AD, Gundersen GW, Fernandez NF, Wang Z, Monteiro CD, McDermott MG, et al. The harmonizome: a collection of processed datasets gathered to serve and mine knowledge about genes and proteins. *Database.* 2016;2016:baw100.
- Pouliquen DL, Boissard A, Coqueret O, Guette C. Biomarkers of tumor invasiveness in proteomics (Review). *Int J Oncol.* 2020;57:409–32.

36. Choi S, Bhagwat AM, Al Mismar R, Goswami N, Ben Hamidane H, Sun L, et al. Proteomic profiling of human cancer pseudopodia for the identification of anti-metastatic drug candidates. *Sci Rep.* 2018;8:5858.
37. Thuault S, Mamelonet C, Salameh J, Ostacolo K, Chanez B, Salaün D, et al. A proximity-labeling proteomic approach to investigate invadopodia molecular landscape in breast cancer cells. *Sci Rep.* 2020;10:6787.
38. Zagryazhskaya-Masson A, Monteiro P, Macé A-S, Castagnino A, Ferrari R, Infante E, et al. Intersection of TKS5 and FGD1/CDC42 signaling cascades directs the formation of invadopodia. *J Cell Biol.* 2020;219:e201910132.
39. Attanasio F, Caldieri G, Giacchetti G, van Horsen R, Wieringa B, Buccione R. Novel invadopodia components revealed by differential proteomic analysis. *Eur J Cell Biol.* 2011;90:115–27.
40. Mueller SC, Artym VV, Kelly T. Invadopodia: interface for invasion. In: Edwards D, Høyer-Hansen G, Blasi F, Sloane BF, editors. *The cancer degradome: proteases and cancer biology.* New York, NY: Springer New York; 2008. p. 403–31.
41. Eble JA, Niland S. The extracellular matrix in tumor progression and metastasis. *Clin Exp Metastasis.* 2019;36:171–98.
42. Havrylov S, Park M. MS/MS-based strategies for proteomic profiling of invasive cell structures. *Proteomics.* 2015;15:272–86.
43. Cervero P, Himmel M, Kruger M, Linder S. Proteomic analysis of podosome fractions from macrophages reveals similarities to spreading initiation centres. *Eur J Cell Biol.* 2012;91:908–22.
44. Kohen R, Barlev J, Hornung G, Stelzer G, Feldmesser E, Kogan K, et al. UTAP: user-friendly transcriptome analysis pipeline. *BMC Bioinform.* 2019;20:154.
45. Martin M. CUTADAPT removes adapter sequences from high-throughput sequencing reads. *EMBnetjournal.* 2011;17:10–12.
46. Dobin A, Davis CA, Schlesinger F, Drenkow J, Zaleski C, Jha S, et al. STAR: ultrafast universal RNA-seq aligner. *Bioinformatics.* 2013;29:15–21.
47. Love MI, Huber W, Anders S. Moderated estimation of fold change and dispersion for RNA-seq data with DESeq2. *Genome Biol.* 2014;15:550.
48. Benjamini Y, Hochberg Y. Controlling the false discovery rate: a practical and powerful approach to multiple testing. *J R Stat Soc Ser B (Methodol).* 1995;57:289–300.
49. Makowiecka A, Simiczyjew A, Nowak D, Mazur AJ. Varying effects of EGF, HGF and TGFβ on formation of invadopodia and invasiveness of melanoma cell lines of different origin. *Eur J Histochem.* 2016;60:2728.
50. Kandasamy S, Adhikary G, Rorke EA, Friedberg JS, Mickle MB, Alexander HR, et al. The YAP1 signaling inhibitors, verteporfin and CA3, suppress the mesothelioma cancer stem cell phenotype. *Mol Cancer Res.* 2020;18:343–51.
51. Liu-Chittenden Y, Huang B, Shim JS, Chen Q, Lee SJ, Anders RA, et al. Genetic and pharmacological disruption of the TEAD-YAP complex suppresses the oncogenic activity of YAP. *Genes Dev.* 2012;26:1300–5.
52. Piccolo S, Dupont S, Cordenonsi M. The biology of YAP/TAZ: hippo signaling and beyond. *Physiol Rev.* 2014;94:1287–312.
53. Janse van Rensburg HJ, Yang X. The roles of the Hippo pathway in cancer metastasis. *Cell Signal.* 2016;28:1761–72.
54. Ou C, Sun Z, Li S, Li G, Li X, Ma J. Dual roles of yes-associated protein (YAP) in colorectal cancer. *Oncotarget.* 2017;8:75727–41.
55. Jho E. Dual role of YAP: oncoprotein and tumor suppressor. *J Thorac Dis.* 2018;10 Suppl 33:S3895–S3898.
56. Zancanato F, Cordenonsi M, Piccolo S. YAP/TAZ at the roots of cancer. *Cancer Cell.* 2016;29:783–803.
57. Yuan M, Tomlinson V, Lara R, Holliday D, Chelala C, Harada T, et al. Yes-associated protein (YAP) functions as a tumor suppressor in breast. *Cell Death Differ.* 2008;15:1752–9.
58. Coffman LG, Burgos-Ojeda D, Wu R, Cho K, Bai S, Buckanovich RJ. New models of hematogenous ovarian cancer metastasis demonstrate preferential spread to the ovary and a requirement for the ovary for abdominal dissemination. *Transl Res.* 2016;175:92–102.e102.
59. Jakubowska M, Sniegocka M, Podgorska E, Michalczyk-Wetula D, Urbanska K, Susz A, et al. Pulmonary metastases of the A549-derived lung adenocarcinoma tumors growing in nude mice. A multiple case study. *Acta Biochim Pol.* 2013;60:323–30.
60. Takahashi K, Ehata S, Koinuma D, Morishita Y, Soda M, Mano H, et al. Pancreatic tumor microenvironment confers highly malignant properties on pancreatic cancer cells. *Oncogene.* 2018;37:2757–72.
61. Shevrin DH, Gorny KI, Kukreja SC. Patterns of metastasis by the human prostate cancer cell line PC-3 in athymic nude mice. *Prostate.* 1989;15:187–94.
62. Jin X, Demere Z, Nair K, Ali A, Ferraro GB, Natoli T, et al. A metastasis map of human cancer cell lines. *Nature.* 2020;588:331–6.
63. Leong Hon S, Robertson Amy E, Stoletov K, Leith Sean J, Chin Curtis A, Chien Andrew E, et al. Invadopodia are required for cancer cell extravasation and are a therapeutic target for metastasis. *Cell Rep.* 2014;8:1558–70.
64. Blouw B, Seals DF, Pass I, Diaz B, Courtneidge SA. A role for the podosome/invadopodia scaffold protein Tks5 in tumor growth in vivo. *Eur J Cell Biol.* 2008;87:555–67.
65. Wei P, Zhao YG, Zhuang L, Ruben S, Sang QX. Expression and enzymatic activity of human disintegrin and metalloproteinase ADAM19/meltrin beta. *Biochem Biophys Res Commun.* 2001;280:744–55.
66. Lizarraga F, Poincloux R, Romao M, Montagnac G, Le Dez G, Bonne I, et al. Diaphanous-related formins are required for invadopodia formation and invasion of breast tumor cells. *Cancer Res.* 2009;69:2792–800.
67. Schirenbeck A, Bretschneider T, Arasada R, Schleicher M, Faix J. The Diaphanous-related formin dDia2 is required for the formation and maintenance of filopodia. *Nat Cell Biol.* 2005;7:619–25.
68. Takkunen M, Hukkanen M, Liljestrom M, Grenman R, Virtanen I. Podosome-like structures of non-invasive carcinoma cells are replaced in epithelial-mesenchymal transition by actin comet-embedded invadopodia. *J Cell Mol Med.* 2010;14:1569–93.
69. Pelaez R, Pariente A, Perez-Sala A, Larrayoz IM. Integrins: moonlighting proteins in invadosome formation. *Cancers.* 2019;11:615.
70. Chellaiah M, Kizer N, Silva M, Alvarez U, Kwiatkowski D, Hruska KA. Gelsolin deficiency blocks podosome assembly and produces increased bone mass and strength. *J Cell Biol.* 2000;148:665–78.
71. Mazurkiewicz E, Makowiecka A, Mrowczyńska E, Koperny I, Nowak D, Mazur AJ. Gelsolin contributes to the motility of A375 melanoma cells and this activity is mediated by the fibrous extracellular matrix protein Profile. *Cells.* 2021;10:1848.
72. Simone TM, Higgins CE, Czekay R-P, Law BK, Higgins SP, Archambeault J, et al. SERPINE1: a molecular switch in the proliferation-migration dichotomy in wound-“activated” keratinocytes. *Adv Wound Care.* 2014;3:281–90.
73. Akakura S, Gelman IH. Pivotal role of AKAP12 in the regulation of cellular adhesion dynamics: control of cytoskeletal architecture, cell migration, and mitogenic signaling. *J Signal Transduct.* 2012;2012:529179.
74. Edgar R, Domrachev M, Lash AE. Gene Expression Omnibus: NCBI gene expression and hybridization array data repository. *Nucleic Acids Res.* 2002;30:207–10.

ACKNOWLEDGEMENTS

We thank the scientific staff at the Department of Life Sciences Core facilities, Weizmann Institute of Science (WIS), for the access to the research infrastructure used in this study, and for their competent help. We are particularly grateful to Dr. Yishai Levin at The De Botton Protein Profiling Institute of the Nancy and Stephen Grand Israel National Center for Personalized Medicine (G-INCPM), WIS, for the scientific input, guidance and help in the proteomic profiling. We are grateful to the Crown Genomics institute of the G-INCPM, WIS, for their assistance in RNA sequencing. We also thank Dr. Shlomit Reich-Zeliger (Prof. Nir Friedman Lab) for assistance with some of the reagents and access to instruments used for RNA quantitation and quality assessment of RNA samples for the RNA sequencing experiments in this study. This study was supported by grants from the Minerva Center for Aging, and a Precision Medicine grant from the Israel Science Foundation.

AUTHOR CONTRIBUTIONS

JBV participated in the design and execution of the experiments included in this study, preparation of the figures and in writing of the manuscript. BD participated in the analysis of the transcriptomic and proteomic data, and in the assembly of the literature-based invadopodia proteome database used here. DM participated in the proteomic profiling of the samples. MSS participated in the experimental design of the YAP/TAZ modulation experiments. MO participated in the experimental design and in the interpretation of the data. BG participated in the design and follow-up of the experiments included in this study, data interpretation and in writing of the manuscript.

COMPETING INTERESTS

The authors declare no competing interests.

ADDITIONAL INFORMATION

Supplementary information The online version contains supplementary material available at <https://doi.org/10.1038/s41419-023-05769-1>.

Correspondence and requests for materials should be addressed to Benjamin Geiger.

Reprints and permission information is available at <http://www.nature.com/reprints>

Publisher's note Springer Nature remains neutral with regard to jurisdictional claims in published maps and institutional affiliations.



Open Access This article is licensed under a Creative Commons Attribution 4.0 International License, which permits use, sharing, adaptation, distribution and reproduction in any medium or format, as long as you give appropriate credit to the original author(s) and the source, provide a link to the Creative Commons license, and indicate if changes were made. The images or other third party material in this article are included in the article's Creative Commons license, unless indicated otherwise in a credit line to the material. If material is not included in the article's Creative Commons license and your intended use is not permitted by statutory regulation or exceeds the permitted use, you will need to obtain permission directly from the copyright holder. To view a copy of this license, visit <http://creativecommons.org/licenses/by/4.0/>.

© The Author(s) 2023